Remote Sensing of Environment 297 (2023) 113763

Contents lists available at ScienceDirect

Remote Sensing of Environment

journal homepage: www.elsevier.com/locate/rse

A robust and flexible satellite aerosol retrieval algorithm for multi-angle polarimetric measurements with physics-informed deep learning method

Minghui Tao [a], Jinxi Chen [a], Xiaoguang Xu [b], Wenjing Man [a], Lina Xu [c,*], Lunche Wang [a], Yi Wang [a], Jun Wang [d], Meng Fan [e], Muhammad Imran Shahzad [f], Liangfu Chen [e]

[a] Hubei Key Laboratory of Regional Ecology and Environmental Change, School of Geography and Information Engineering, China University of Geosciences, Wuhan 430074, China
[b] Joint Center for Earth Systems Technology and Department of Physics, University of Maryland Baltimore County, Baltimore, MD 21250, USA
[c] Subsurface Multi-scale Imaging Key Laboratory, School of Geophysics and Geomatics, China University of Geosciences, Wuhan 430074, China
[d] Dept. of Chemical & Environmental Engineering, University of Iowa, Iowa City 52242-1503, USA
[e] State Key Laboratory of Remote Sensing Science, Aerospace Information Research Institute, Chinese Academy of Sciences, Beijing 100101, China
[f] Earth & Atmospheric Remote Sensing Lab, Department of Meteorology, COMSATS University Islamabad, Islamabad 45550, Pakistan

ARTICLE INFO

Edited by Dr. Menghua Wang

Keywords:
Aerosols
Multi-angle polarization
POLDER-3
Retrieval algorithm

ABSTRACT

The multi-angle polarimetric (MAP) satellite measurements provide abundant information concerning aerosol optical/microphysical properties. In this study, we present a robust and flexible aerosol retrieval algorithm for MAP measurements based on physics-informed deep learning (PDL) method. Different from optimized inversion that needs iterative Radiative Transfer (RT) calculations of all the unknowns, the PDL method can model the whole MAP observations with each retrieved aerosol parameter separately with the pre-training of RT simulations. Furthermore, the training of PDL can make full use of the prior information from ground-based aerosol inversions and satellite surface products, and provides an effective constraint to avoid unphysical values. To examine performance of PDL algorithm, we retrieve aerosols over eastern China from POLDER-3 measurements during 2007–2009. Comparison with AERONET products shows high correlations ($R > 0.91$) for both POLDER-3 PDL Aerosol Optical Depth (AOD) and fine AOD. Despite lower correlations caused by a small portion of poor retrievals, PDL coarse AOD and Single Scattering Albdeo (SSA) is very consistent with AERONET results. Also, PDL retrievals perform well as the best estimates of optimized methods such as GRASP (Generalized Retrieval of Aerosol and Surface Properties). With an outstanding performance in accuracy and efficiency, the flexible PDL algorithm exhibits great potential for operational retrieval of MAP satellite measurements.

1. Introduction

Atmospheric aerosols play a crucial role in the Earth's climate, air quality and public health (Kaufman et al., 2002; Pope et al., 2002). As a complex mixture originating from diverse emission sources including both nature processes and anthropogenic activities, these particles have different sizes, shapes, and chemical components. Owing to a short lifetime spanning a few hours to several days, the concentration and properties of atmospheric aerosols have large variations over space and time and are subject to dynamic meteorological cycles. By now, accurate estimation of aerosols' effects remains a challenge in associated climate and air quality studies at regional and global scales (Chen et al., 2022a; Forster et al., 2021). Moreover, aerosols are a primary source of uncertainties in satellite remote sensing of greenhouse gases and surface properties in visible and shortwave infrared bands (Sanghavi et al., 2020). Therefore, global observation of aerosols is a fundamental requirement for exploring their emissions and corresponding climate and environmental effects.

The necessity of global aerosol observations has motivated a series of dedicated satellite instruments such as Moderate-resolution Imaging Spectroradiometer (MODIS), Multi-angle Imaging Spectroradiometer (MISR), and Polarization and Directionality of the Earth's Reflectances (POLDER) since late 1990s (King et al., 1999). Since satellite observations can hardly infer all the unknowns of the coupled atmosphere and surface, how to make full use of the distinct information content from different satellite measurements has been the key question of aerosol

* Corresponding author at: NO. 388, Lumo Road, Hongshan District, Wuhan 430074, China.
E-mail addresses: taomh@cug.edu.cn (M. Tao), xulina@cug.edu.cn (L. Xu).

https://doi.org/10.1016/j.rse.2023.113763
Received 28 April 2023; Received in revised form 20 July 2023; Accepted 11 August 2023

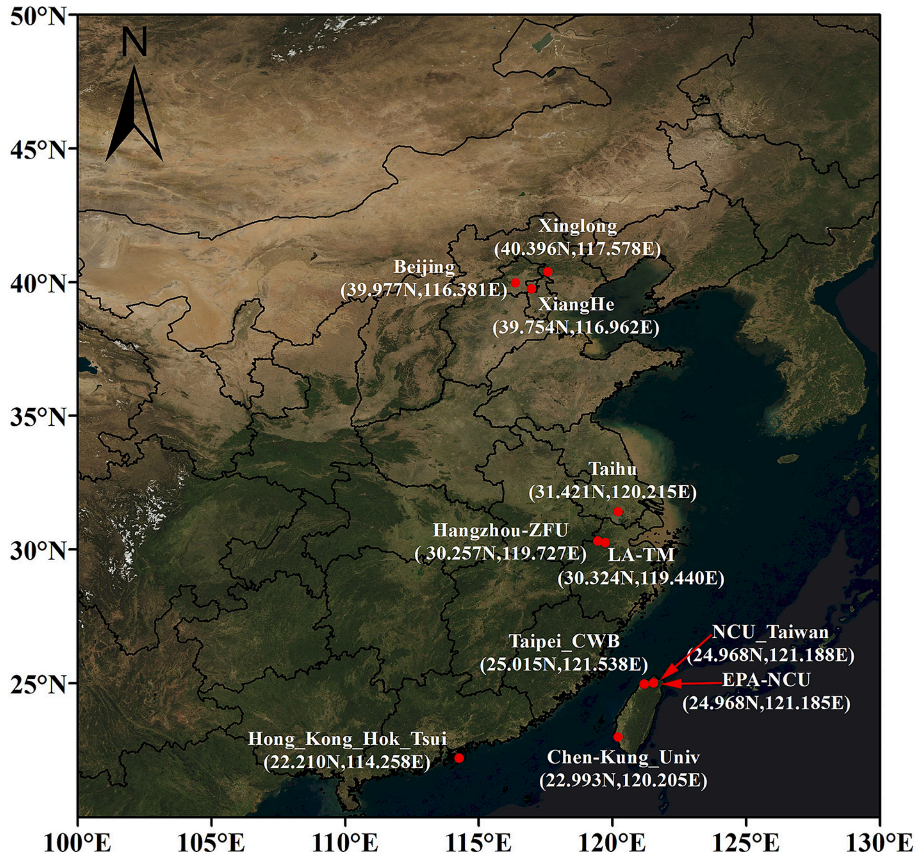

Fig. 1. a) Geographic location of AERONET sites (red) in MODIS true color image of eastern China. (For interpretation of the references to color in this figure legend, the reader is referred to the web version of this article.)

remote sensing (Xu and Wang, 2015). For multi-spectral or multi-angle measurements, MODIS and MISR algorithms utilize fixed aerosol models or their mixtures pre-calculated in look-up tables (LUT) (Hsu et al., 2013; Levy et al., 2013; Lyapustin et al., 2018; Kahn and Gaitley, 2015). Despite an advantage of simplicity and efficiency, the LUT-based retrievals are usually subject to the large spatial and temporal variations of aerosol properties (Tao et al., 2019, 2020).

By contrast, the multi-angle polarimetric (MAP) measurements from POLDER with abundant information content make it possible to retrieve more aerosol optical/microphysical properties. By fitting MAP measurements with iterative online RT calculations under prior constraint, the usually used optimized inversion methods can simultaneously retrieve aerosol and surface parameters (Dubovik et al., 2011; Hasekamp et al., 2011; Waquet et al., 2009; Xu et al., 2017). The recent GRASP (Generalized Retrieval of Aerosol and Surface Properties) and SRON RemoTAP (Remote Sensing of Trace gas and Atmosphere Products) algorithm have achieved great advancements in MAP retrieval of particle size and absorption (Chen et al., 2020; Fu and Hasekamp, 2018; Li et al., 2019, 2022). More advanced MAP instruments such as Multi-Angle Imager for Aerosols (MAIA) and Multi-Viewing Multi-Channel Multi-Polarization Imaging (3MI) have been in plan to enhance global observation of aerosol and greenhouse gases (Diner et al., 2018; Fougnie et al., 2018).

Since optimized inversions need iterative RT calculations of all aerosol/surface unknowns together, aerosol or surface parameters with low information content in satellite measurements can transmit their uncertainties to the whole retrievals (Dubovik et al., 2019; Xu and Wang, 2015). Moreover, future MAP instruments such as MAIA and 3MI have more spectral and polarimetric bands, higher spatial resolution, and larger swath width (Diner et al., 2018; Fougnie et al., 2018). The huge increase in MAP measurement information and data volume have exerts a very high requirement on computational efficiency of aerosol algorithms to implement operational retrievals.

With the powerful non-linear modeling ability and high computational efficiency, the Deep Learning (DL) methods have been increasingly utilized in both forward RT calculations and satellite retrievals (Chen et al., 2022b; Di Noia et al., 2015). By training relationship between spectral reflectance at top of atmosphere (TOA) with ground-based observations using DL methods, satellite retrievals of AOD and fine mode fraction exhibit a good accuracy (Kang and Kim, 2022). Nevertheless, performance of these data-driven DL retrievals relies on the availability and representativeness of ground observations. On the other hand, RT simulations are trained by DL methods to accelerate optimized estimation or to construct functions of satellite TOA reflectance and AOD (Jia et al., 2022; Shi et al., 2020). In particular, exploratory study from airborne MAP observations shows that aerosol microphysical parameters can be well retrieved by training RT simulations with DL methods (Gao et al., 2021; Di Noia et al., 2017). By now, whether DL methods can improve the current optimized inversion of MAP satellite measurements has been rarely concerned.

In this study, we present a robust and flexible retrieval algorithm for aerosol optical/microphysical properties from MAP satellite measurements by combining the advantages of physical constraints from atmospheric RT simulations and modeling ability of DL methods. Section 2 gives a brief introduction of POLDER-3 and AERONET (Aerosol Robotic Network) measurements and their products. The whole framework of our aerosol retrieval algorithm is introduced in section 3. Then, performance of our algorithm are analyzed by ground-based validation and inter-comparison with existing satellite products in section 4. Section 5 summarizes the main conclusions.

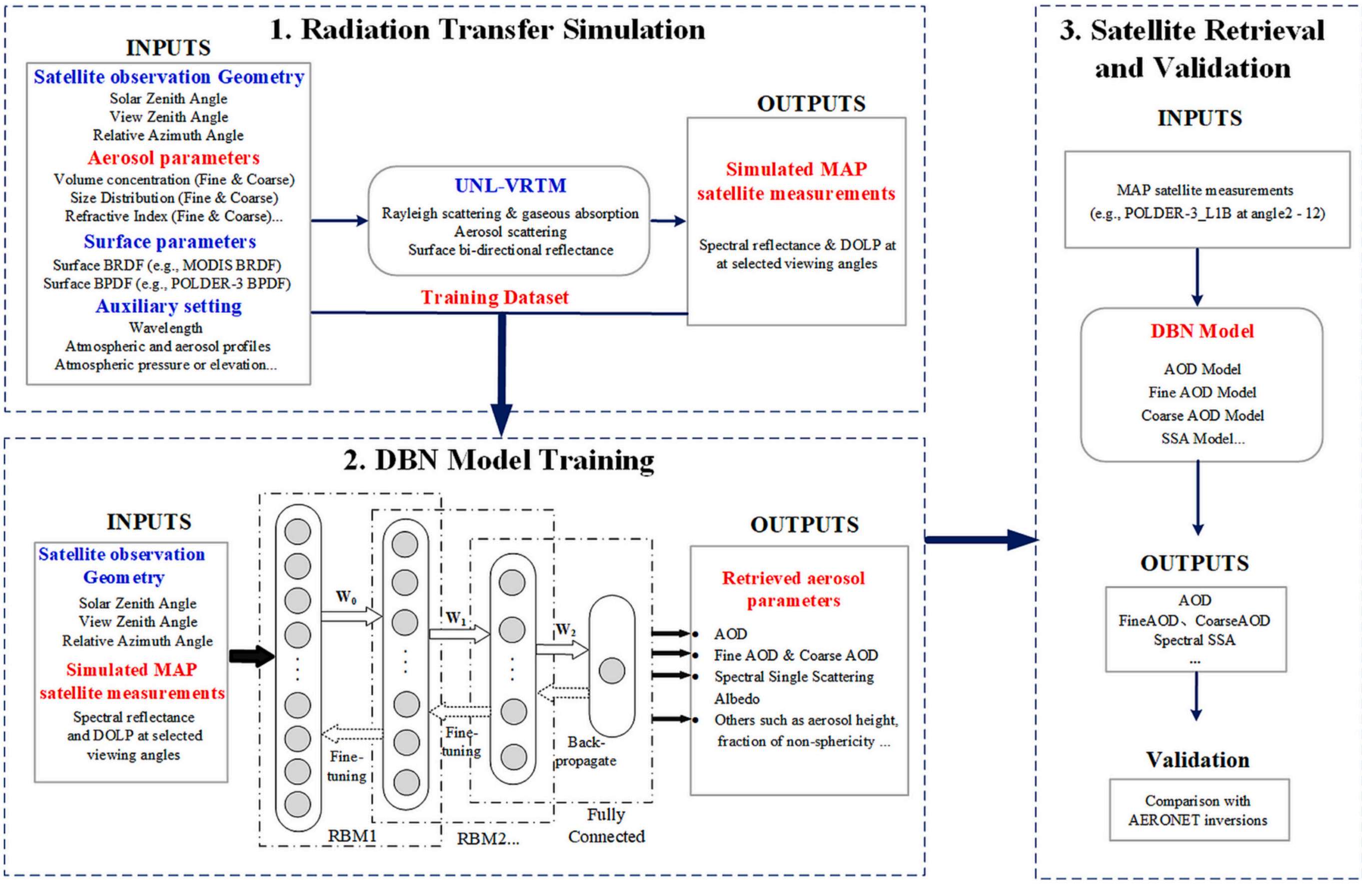

Fig. 2. The flowchart of PDL aerosol algorithm for multi-angle polarimetric measurements.

2. Satellite and ground measurements

2.1. POLDER-3 data

The POLDER instrument crossing the equator at 13:30 local time measures the intensity and polarization of backscattered sunlight of the Earth-atmosphere system with 9 spectral bands from different view directions (up to 14–16 viewing angles). While POLDER 1–2 instruments onboard ADEOS satellites since 1996 and 2002 have a limited lifespan of 8 and 7 months, POLDER-3 on the PARASOL satellite from December 2004 operates up to the end of 2013 (Tanré et al., 2011). With a swath width of 1600 km and nadir spatial resolution of ~6 km, POLDER-3 measures scattering intensity of aerosols and clouds at 6 channels (443, 490, 565, 670, 865 and 1020 nm) with additional polarimetric observations at 490, 670, 865 nm. Moreover, the other three channels (763, 765 and 910 nm) are used to measure gaseous absorption of oxygen A-band and water vapor. We utilize degree of linear polarization (DOLP) for aerosol retrieval, a relative quantity with higher accuracy than polarized radiance or reflectance:

$$DOLP = \frac{\sqrt{Q^2 + U^2}}{I} \tag{1}$$

Here I, Q, and U are the first three of the Stoke parameters. Considering some values are missing in large viewing angles, only POLDER-3 measurements at viewing angles 2–12 are selected in our retrieval.

As an optimized algorithm without LUTs, GRASP can simultaneously retrieve aerosol and surface properties (Dubovik et al., 2021). According to different configurations and assumptions, POLDER-3/GRASP has four types of retrievals: Optimized, Optimized with High-Precision (HP) RT calculation, Models, and Components. By assuming fine and coarse aerosols have the same component, GRASP/HP retrievals include volume size distribution at five bins, spectral complex refractive index, fractions of spherical particles, aerosol layer height (ALH), surface bidirectional reflectance distribution function (BRDF) and bidirectional polarization distribution function (BPDF) parameters (Dubovik et al., 2011). GRASP/Models method takes aerosols as an external mixture of several aerosol components, and their respective concentrations together with ALH and surface parameters are retrieved (Chen et al., 2020). By contrast, internal mixture of several components in fine and coarse mode separately is utilized in GRASP/Components with similar retrievals (Li et al., 2019). Meanwhile, a priori constraints such as BRDF/BPDF are spectrally smooth are utilized. While ground validations of GRASP/HP aerosol microphysical parameters show reliable accuracy, GRASP/Moldes performs better in the total AOD retrieval (Chen et al., 2020; Li et al., 2022; Zhang et al., 2021). Here we select these POLDER-3 GRASP products with quality-assured filtering for intercomparison with our retrievals.

2.2. AERONET measurements

AERONET is a ground-based aerosol remote sensing network established since 1990s, which provides long-term and continuous aerosol observation with well-calibrated sun-sky photometers (Holben et al., 1998). By measuring direct solar irradiance every 5–15 min, spectral AODs derived from AERONET observations have a very high accuracy (~0.01–0.02) (Giles et al., 2019). Combined with directional almucantar observations of sky radiance at 440, 675, 870 and 1020 nm, AERONET operational inversion retrieves 22 bins of particle size distribution, spectral, and nonsphericity with similar optimized method as POLDER-3/GRASP (Dubovik and Holben, 2002). To ensure a reliable accuracy, quality control of AERONET complex refractive index requires

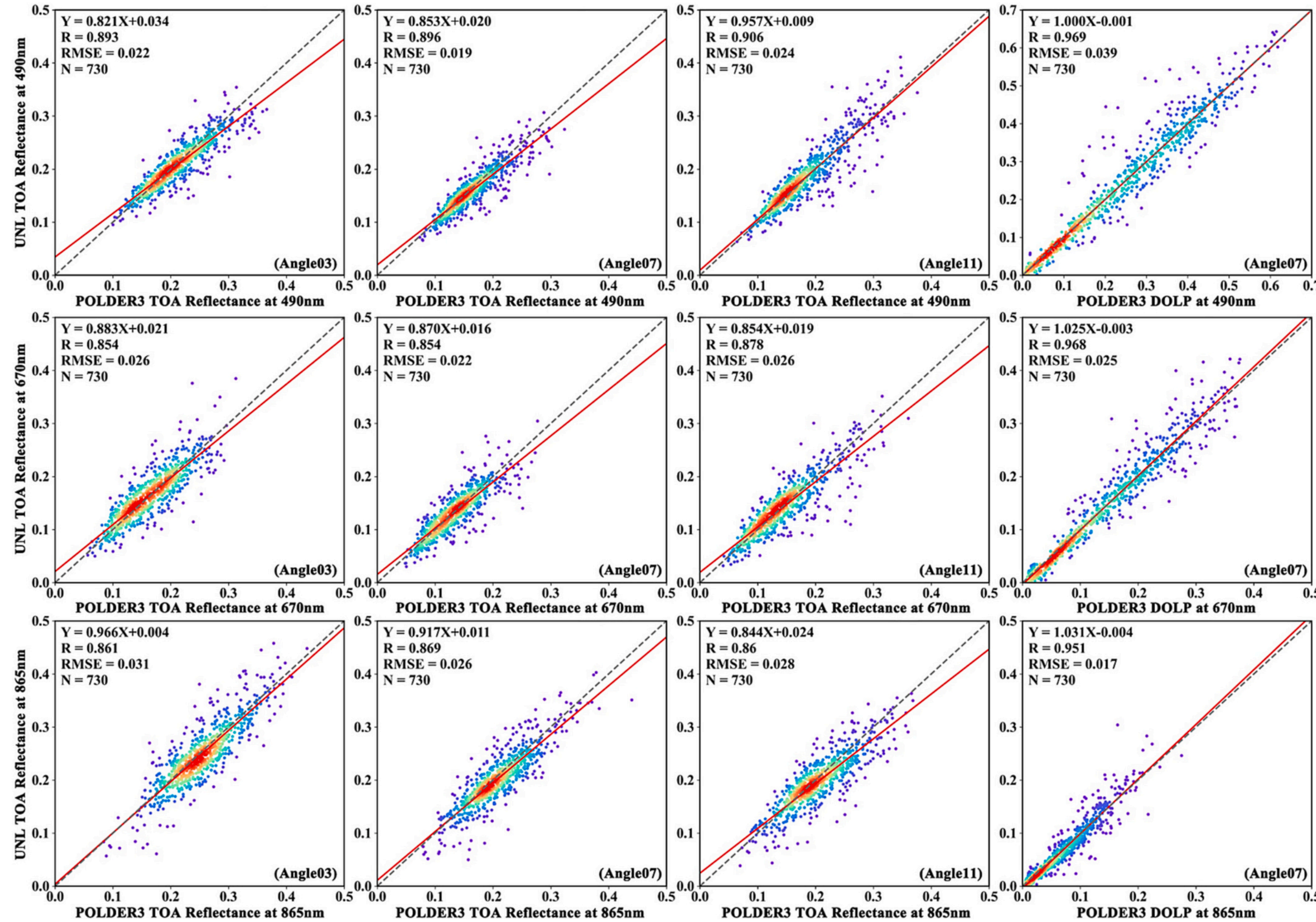

Fig. 3. Comparison of RT simulations of TOA spectral reflectance and DOLP with corresponding POLDER-3 measurements at 490, 670 and 865 nm for typical viewing angles. The red and dashed lines are fitting and 1:1 lines. Correlation coefficient (R), Root Mean Square Error (RMSE), and number (N) of simulation-measurement matchups are also shown. (For interpretation of the references to color in this figure legend, the reader is referred to the web version of this article.)

$AOD_{440} > 0.4$ and solar zenith angle (SZA) $>50^\circ$. The Version (V) 3 AERONET inversions introduce a new hybrid sky measurement to maximize the range of scattering angles, and extend the threshold of SZA to 25° (Sinyuk et al., 2020). Surface reflectance has minimal influence on AERONET sky radiance, and is considered with MODIS BRDF products.

We select the V3 AERONET Level 2.0 products for the validation of our retrievals. Consistent with previous studies (Chen et al., 2020; Ichoku et al., 2002), spatial mean values of POLDER-3 retrievals within a radius of ~25 km around AERONET site are matched with temporal mean of AERONET observations within ±30 min of satellite passing time. For microphysical parameters such as complex refractive index, the temporal window is expanded to ±1 h. Fig. 1 shows locations of the 11 AERONET sites used in this study.

3. MAP aerosol retrieval with physics-informed DL (PDL) method

A reliable atmospheric RT model can provide a high-accuracy calculation of satellite TOA reflectance and DOLP from the coupled atmosphere and surface system at various viewing geometries. Thus, a clear physical mapping relationship exists between simulated MAP measurements and corresponding RT inputs (aerosol optical/microphysical parameters and surface BRDF/BPDF). Then, a DL method can be utilized to train the complicated non-linear relationship between MAP satellite measurements and aerosol parameters. Different from optimized inversion depending on absolute physical quantities, DL methods make feature learning of probability distribution of the training datasets. Furthermore, with the physical constraints of RT simulations, DL method can model the whole used MAP measurement with each aerosol parameter separately without having to retrieve all aerosol/surface unknowns together.

3.1. Atmospheric RT model

The UNified and Linearized Vector Radiative Transfer Model (UNL-VRTM) is a numerical testbed for atmospheric remote sensing (Wang et al., 2014), which is mainly composed of several modules including a linearized vector radiative transfer model (VLIDORT), aerosol scattering (Mie/T-Matrix code), Rayleigh scattering and gas absorption, and surface reflectance model (BRDF/BPDF). UNL-VRTM supports a flexible setting of the functions such as aerosol size distribution, vertical profiles, and surface BRDF/BPDF models. Up to two aerosol modes and their respective loading (AOD or volume concentration) and microphysical properties (particle size and complex refractive index) can be inputted. Spherical aerosols with a bimodal lognormal distribution are assumed in this study:

$$\frac{dV}{d\ln r} = \sum_{i=1}^{2} \frac{V_0^i}{\sqrt{2\pi} ln\sigma_g^i} exp\left[-\frac{\left(lnr - lnr_v^i\right)^2}{2ln^2\sigma_g^i}\right] \tag{2}$$

V_0 denotes total volume concentration ($\mu m^3 \mu m^{-2}$); the superscript i = 1, 2 refers to fine and coarse mode aerosols with assumed size range of

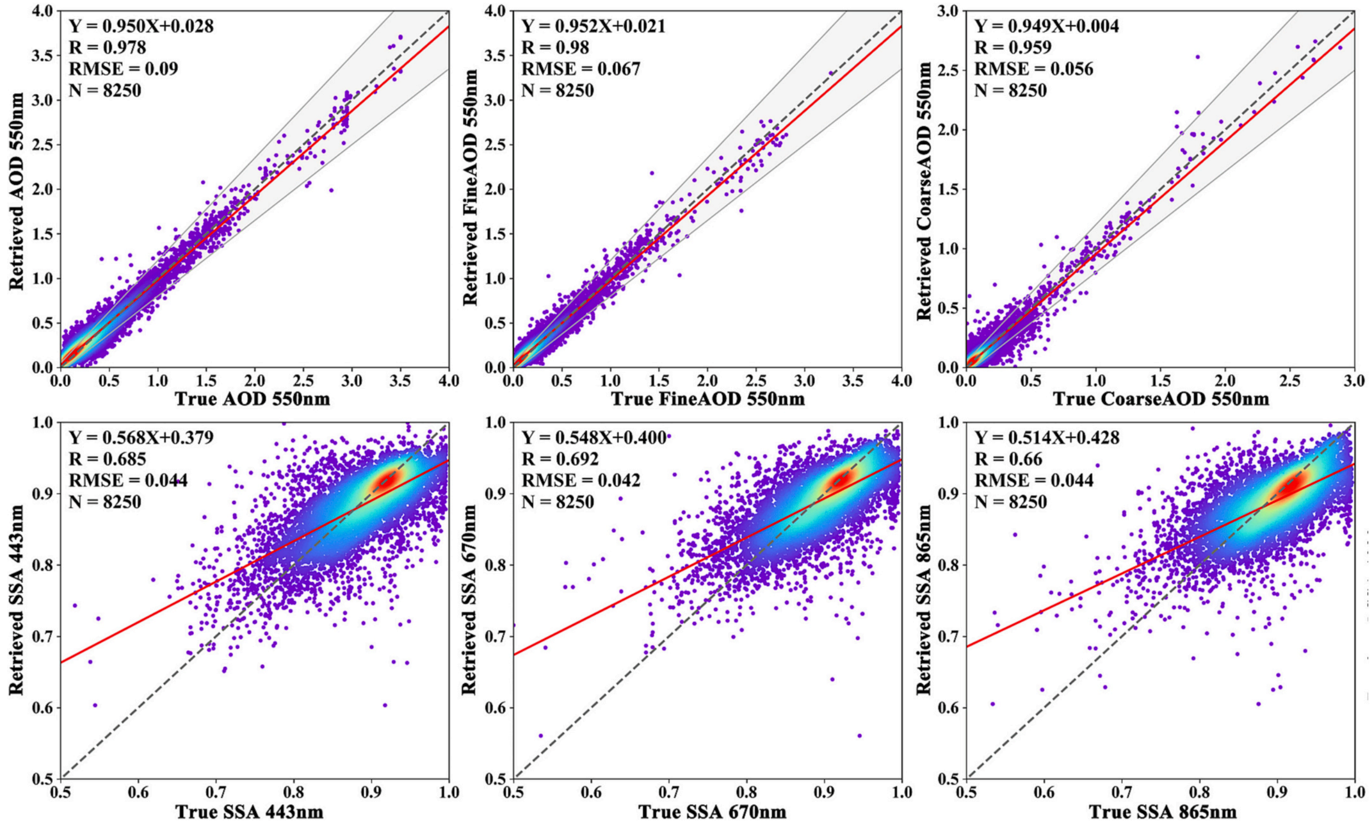

Fig. 4. The comparison of PDL retrievals and true values of AOD, fine AOD, coarse AOD at 550 nm, and SSA at 443, 670 and 865 nm from synthetic test data. The black and dashed lines are expected error (EE) envelop of ±(0.05 + 15%) and 1:1 line.

0.01–10 μm and 0.05–20 μm respectively, which both cover >99.9% of the idealistic particle sizes. r_v and σ_g represent volume median radius and its geometeic standard deviation. Effective radius (r_{eff}) can be calculated by r_v and σ_g:

$$r_{eff} = r_v exp\left(-\frac{1}{2}ln^2\sigma_g\right) \tag{3}$$

Then AOD (τ_a) at a specific wavelength (λ) can be obtained:

$$\tau_a(\lambda) = \sum_{i=1}^{2} \frac{3V_0^i Q_{ext}^i(\lambda)}{4r_{eff}^i} \tag{4}$$

The extinction efficiency factor, Q_{ext}, is the ratio of extinction and geometric cross section. For surface BRDF, we select a widely used semiempirical model that relies on a linear weighted sum of isotropic scattering, Ross-Thick volume scattering (K_{vol}), and

$$R(\lambda, \vartheta_0, \vartheta_v, \varphi) = f_{iso}(\lambda) + f_{vol}(\lambda)K_{vol}(\vartheta_0, \vartheta_v, \varphi) + f_{geo}(\lambda)K_{geo}(\vartheta_0, \vartheta_v, \varphi) \tag{5}$$

Li-Sparse geometric scattering (K_{geo}) (Lucht and Schaaf, 2000). f_{iso}, f_{vol}, and f_{geo} are spectrally-dependent weighting parameters. Here ϑ_0, ϑ_v and φ are solar zenith, view zenith, and relative azimuth angles. Since BPDF has very little variations with surface types, we select a fixed model with only one parameter (Maignan et al., 2009).

3.2. Deep Belief Network (DBN)

As one of the competitive and effective Deep Neural Networks (DNN) methods, DBN with a probabilistic generative model has a striking advantage in solving complicated and non-linear regression questions. By combing stacked Restricted Boltzmann Machine (RBM) and a Back-Propagation net (BP), DBN firstly starts an unsupervised pre-training of each RBM and then makes a supervised fine-tuning of its parameters with error back-propagation algorithms (Hinton et al., 2006). RBM is a type of generative stochastic neural network that does feature learning of probability distribution of the input datasets. The typical two-layer neural network of RBM contains a visible layer to input the training data and a hidden layer as feature detectors with connections between but not within layers. Thus, the hidden units in each RBM layer can be trained efficiently to capture higher-order features of the datasets from visible layer using contrastive divergence method. After a layer-by-layer greedy training of the RBMs, the generative weights are restricted in a favorable scope for global training and provide a reliable initial guess for the following supervised fine-tuning. In this study, we utilize DBN method to model the physics-informed relationship among MAP measurements, aerosol, and surface from RT simulations.

3.3. The PDL aerosol algorithm framework

As shown in Fig. 2, PDL algorithm framework includes three key modules: 1) generating training datasets with RT simulations; 2) modeling the relationship between simulated MAP measurements and each interested aerosol parameter separately with DBN; 3) POLDER-3 aerosol retrieval with the trained models. The detailed process of each module is as follows:

(1) First, UNL-VRTM is used to generate the training datasets by simulating POLDER-3 TOA reflectance at six bands (443, 490, 565, 670, 865 and 1020 nm) and DOLP at three polarized ones (490, 670, 865 nm) as used in GRASP inversions under various atmospheric and surface conditions. The aerosols are assumed to be a mixture of fine and coarse mode with dynamic sizes. Volume concentration, effective radius, effective variance, and spectral complex refractive index of each mode are the main input aerosol variables for RT simulation. Aerosol profiles are assumed to follow a fixed Gaussian distribution with AOD peak at ~1.5 km. For atmospheric profiles, the mid-latitude summer and winter

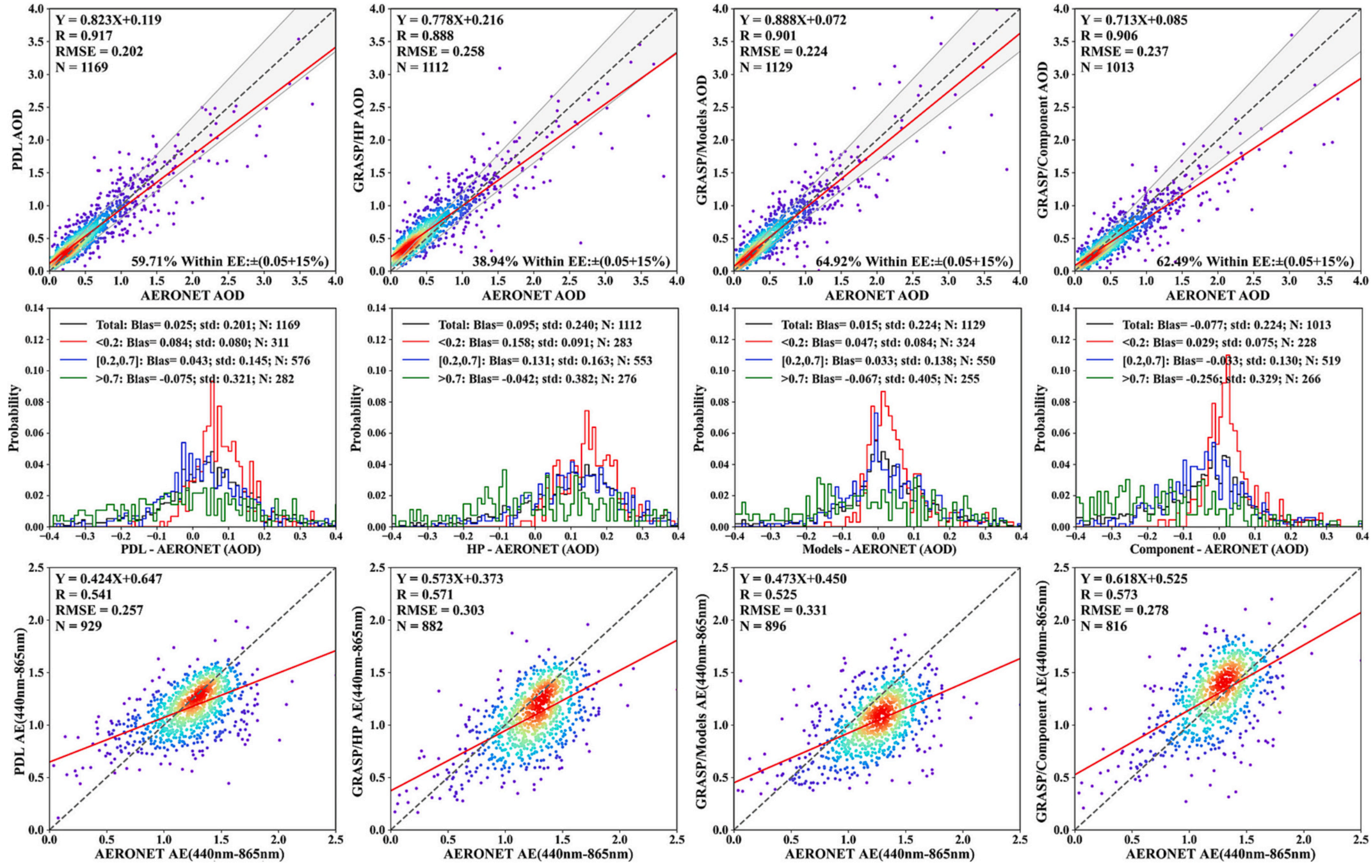

Fig. 5. Ground-based validations of POLDER-3 PDL, GRASP/HP, GRASP/Models, and GRASP/Component AOD with AERONET results at 550 nm (top), probability density functions of their bias (POLDER-AERONET) (middle), and Ångström exponent (AE) at 440–865 nm (bottom).

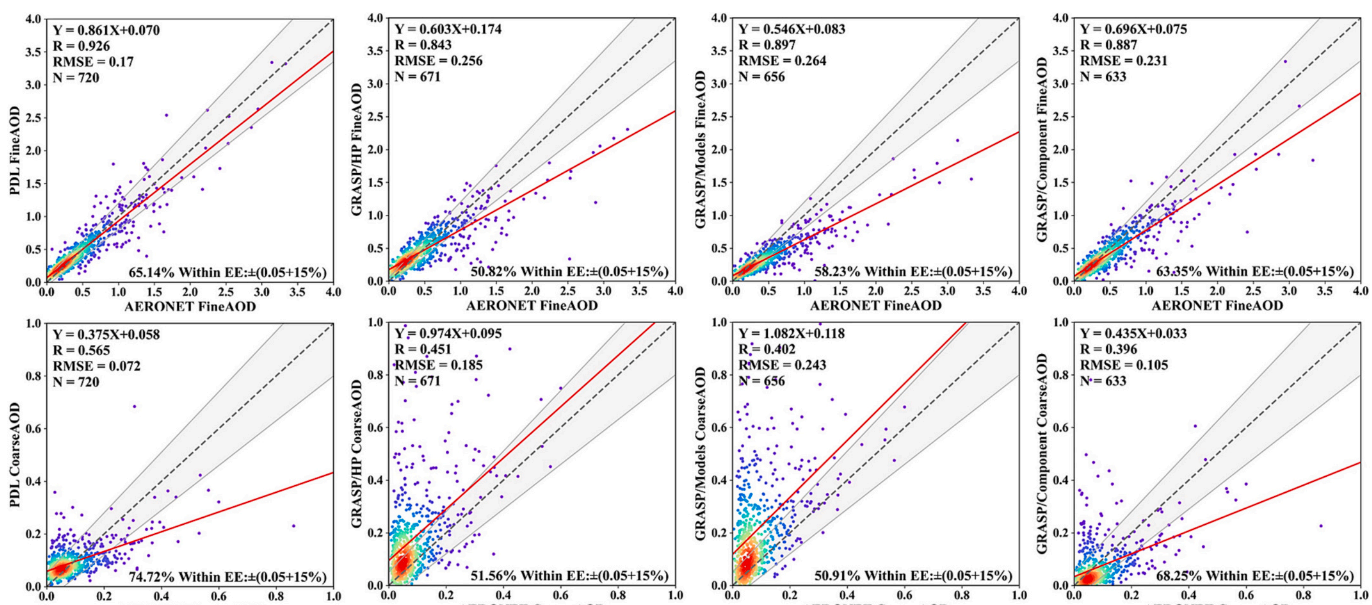

Fig. 6. Same as Fig. 5 but for validation of PDL fine AOD (top) and coarse AOD (bottom).

ones are utilized for simulations at close time respectively.

Since random combinations of aerosol or surface parameters can generate numerous factitious samples that do not exist in the real world, we make use of the prior information from existing ground measurements and satellite products. The AERONET site in Beijing is influenced by local urban/industrial emissions, long-range transport of airborne dust and fire smoke as well as their mixtures. Considering the same complex refractive index is assumed for fine and coarse particles in AERONET inversion, we retrieve their respective microphysical parameters from 10-year (2011−2021) Sun photometer observations in

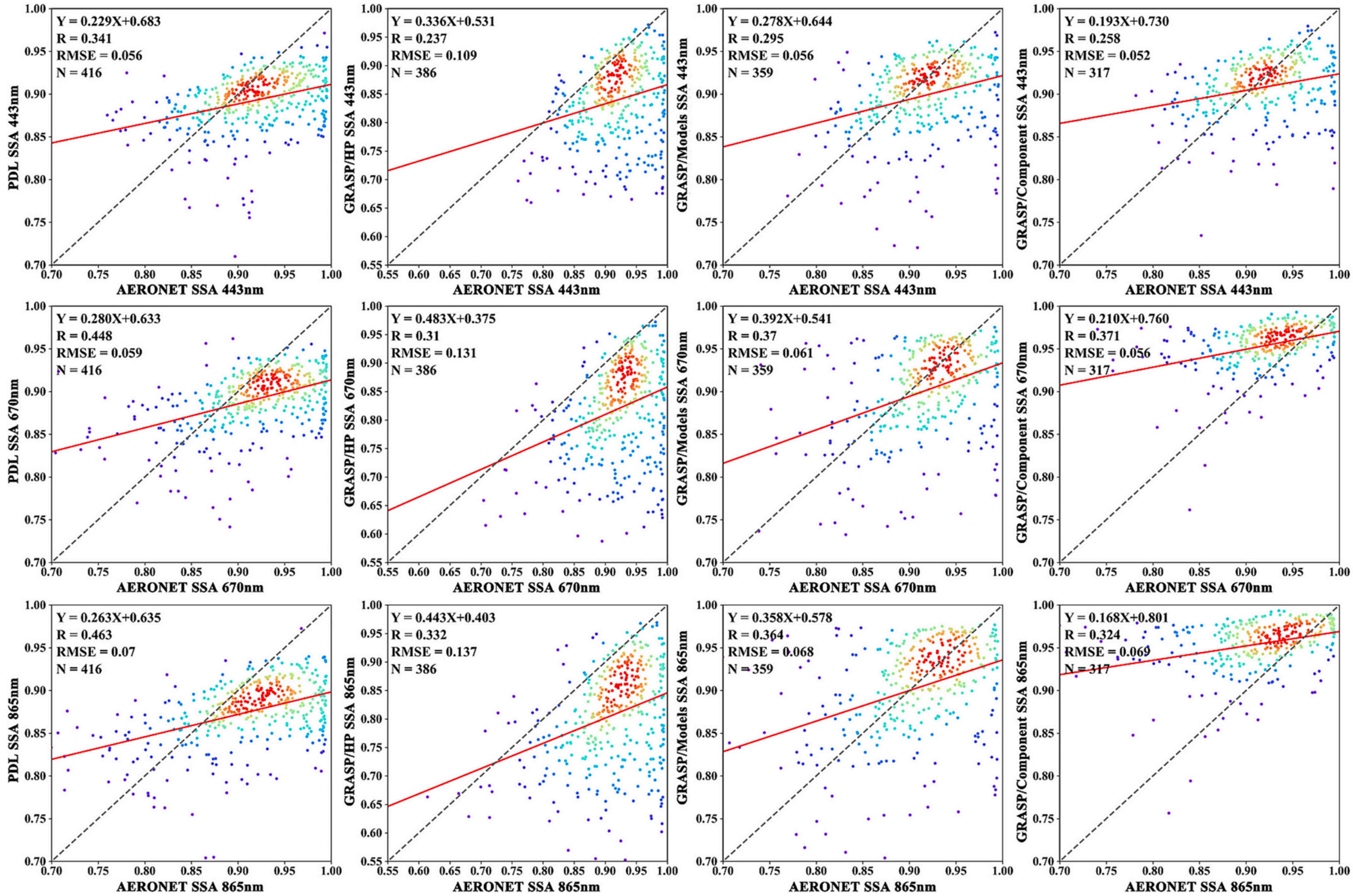

Fig. 7. Scattered plots of POLDER-3 PDL, GRASP/HP, GRASP/Models, and GRASP/Component SSA and AERONET inversions at 443, 670, and 865 nm.

Beijing site with an optimized algorithm by Xu et al. (2015). Moreover, we select one-year collocated MODIS Deep Blue AOD, BRDF, and POLDER-3 BPDF in eastern China during 2007 to combine with the aerosol microphysical parameters. Compared with POLDER-3 measurements, UNL-VTRM simulations in AERONET Beijing site show a robust and reliable performance (Fig. 3). Both simulated TOA reflectance and DOLP are closely concentrated along the 1:1 line with matched single-pixel POLDER-3 measurements, and their correlation coefficients are ranging within 0.854–0.967. It should be stated that DBN makes feature learning of probability distribution functions of the training datasets rather than calculates absolute physical quantities, which has good generalization and anti-noise capabilities and can learn features from even raw data.

(2) The RT simulations from UNL-VTRM provide a physics-informed training dataset between MAP measurement and aerosols. Considering there are too many unknowns of the fine and coarse mode aerosols, we convert their optical/microphysical parameters to AOD, fine and coarse AOD, and Single Scattering Albedo (SSA), which are also the main products of GRASP. It should be noted that here simulated MAP measurements are taken as input and aerosol parameters are taken as unknown output. The observation geometry is still an input as constraint condition. Then, we train the function relationship of simulated POLDER-3 TOA reflectance and DOLP with corresponding AOD, fine and coarse AOD at 550 nm, and spectral SSA using DBN method, respectively. A 20% subset of the sample datasets that does not participate in the training is selected randomly as test dataset to validate the trained models.

It should be noted that here we only train and retrieve aerosols. Different from optimized inversions that need iterative RT calculations of all aerosol/surface unknowns together, PDL method directly models satellite measurements with each retrieved parameter respectively. Surface parameters need to be modeled with satellite measurements separately by PDL method if required. With the full physical constraints among satellite observations, aerosol, and surface in RT simulations, retrieval accuracy of surface properties mainly depends on their information content.

Fig. 4 shows comparison of PDL retrievals from the test dataset with the "true" values of aerosol optical/microphysical parameters. Based on the trained DBN models, PDL AOD, fine and coarse AOD exhibits a very high accuracy with correlation coeffients (R) >0.95. Despite a lower R, most PDL SSA values are well concentrated along 1:1 lines of retrievals and true values.

(3) By utilizing the trained DBN models, we make retrieval of corresponding aerosol parameters from single-pixel POLDER-3 measurements over eastern China during 2007–2009. Considering PDL algorithm does not depend on absolute physical quantities, we do not make quality control for our retrievals.

4. Results and analysis

4.1. Validation of PDL aerosol retreivals from POLDER-3 measurements

To evaluate the retrieval accuracy of PDL algorithm in eastern China, we make a validation of POLDER-3 PDL AOD and GRASP/HP, Models, and Component retrievals with AERONET products (Fig. 5). The POLDER-3 PDL AOD agrees very well with AERONET results with a slightly higher correlation coefficient ($R = 0.917$) and lower Root Mean Square Error (RMSE = 0.202) than GRASP results. On the other hand, percent of PDL AOD (59.71%) within expected error (EE) envelope of $\pm(0.05 + 15\%)$ is lower than that of GRASP/Models (64.92%), which is

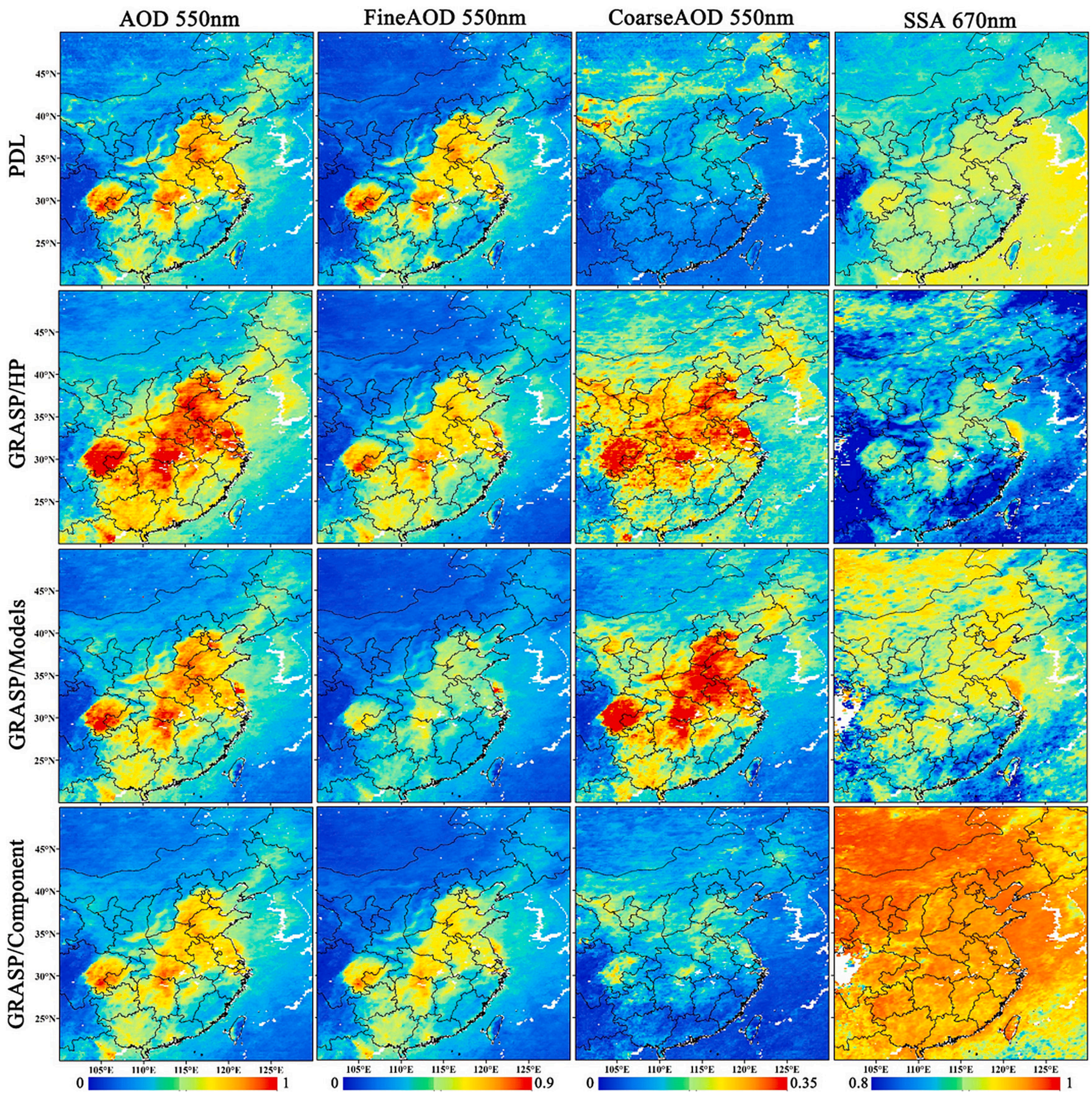

Fig. 8. Annual mean of POLDER-3 AOD, fine AOD, coarse AOD at 550 nm, and SSA at 670 nm for PDL, GRASP/HP, GRASP/Models, and GRASP/Component algorithm in eastern China during 2008.

mainly caused by the overestimation under low-AOD (<0.2) conditions. By contrast, the bias of PDL AOD (>0.2) relative to AERONET observations generally follows a similar Gaussian distribution as that of GRASP/Models. The POLDER-3 PDL Ångström exponent (AE) values at 440–865 nm are concentrated along the 1:1 line, indicating high consistency between spectral AODs from different DBN models.

Meanwhile, POLDER-3 PDL retrievals exhibit a good accuracy in inferring particle size (Fig. 6). Compared with the total AOD, PDL algorithm has a more significant advantage in the retrieval of fine AOD. Ground-based validation with AERONET products shows a high accuracy of PDL fine AOD with $R = 0.926$ and RMSE = 0.17. Moreover, percent of PDL fine AOD within EE exceeds 65%, which is higher than that of GRASP/Models (58.23%) and Component (63.35%). Despite a large decrease in the accuracy of coarse AOD for both GRASP and PDL, PDL retrievals are more reliable with $R = 0.565$ and RMSE = 0.072 and have much fewer abnormal values with 74.72% values within EE of $\pm(0.05 + 15\%)$. GRASP/HP and Models retrievals tend to overestimate coarse AOD with a few abnormally high values. By comparison, GRASP/Component has a lower $R = 0.396$ but better RMSE (0.105) with 68.25% retrievals within EE.

POLDER-3 PDL retrievals of spectral SSA exhibit consistent variations with AERONET inversions (Fig. 7). Different from global validations (Chen et al., 2020), GRASP/Models retrievals of SSA obviously perform better than GRASP/HP and Component results in eastern China. Despite R and RMSE of PDL SSA is at very close levels with those of GRASP/Models retrievals in AERONET validation, GRASP/Models SSA is closer to 1:1 lines. PDL retrievals tend to underestimate high-SSA (>0.90) and overestimate low-SSA (<0.90) values. The complex refractive index of fine and coarse mode aerosols is retrieved separately from AERONET measurements, and then converted to SSA of the total aerosols for PDL training. Information content of coarse particles is lower than that of fine mode aerosols in AERONET measurements (Xu and Wang, 2015). Since fine mode aerosols are predominant in eastern China (Fig. 6), the limited information content of coarse particles with low values (<0.2) further leads to considerable uncertainties in retrieval of their refractive index (Dong et al., 2023), Which can be the main source of the bias in PDL SSA.

Generally, the PDL algorithm exhibits a robust and reliable performance in retrieving aerosol optical/microphysical parameters from POLDER-3 measurements. Compared with optimized inversions, accuracy of PDL retrievals is at very close levels with the best one of the three GRASP products, and possess marked advantage in characterizing

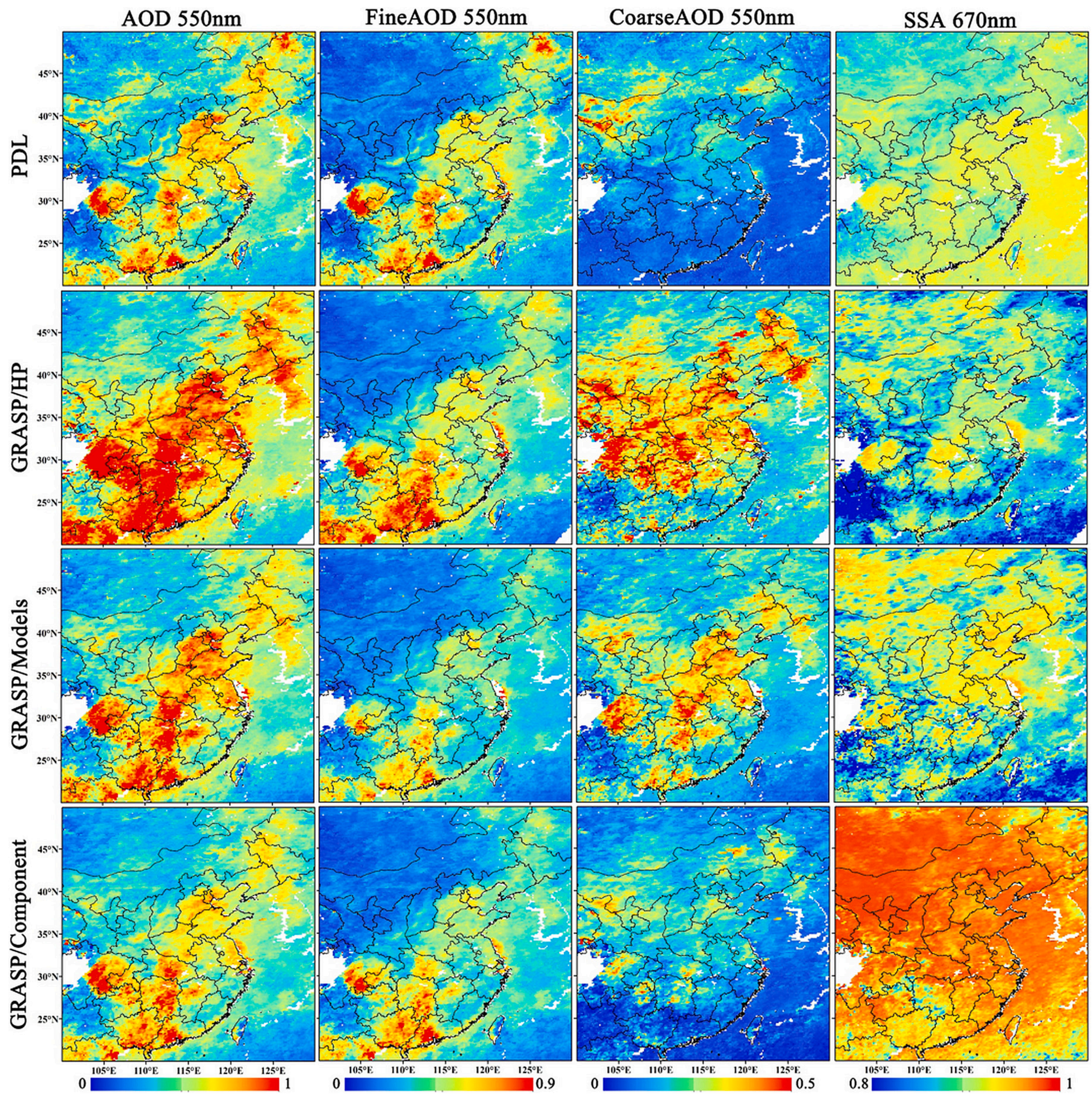

Fig. 9. Same as Fig. 8 but for seasonal mean during spring in 2008.

particle size. Also, PDL method can make full use of the prior information of aerosol/surface parameters from ground-based observations and satellite products, which can avoid very abnormal values. With the physical constraints among satellite measurements, aerosol, and surface from RT simulations, aerosol/surface parameters can be selected flexibly and modeled with the whole MAP measurements separately with a high utilization efficiency of observational information. In particular, the PDL method has a very high computational efficiency at minute level on average for retrieval of one POLDER-3 image using common persional computers (PC).

4.2. Inter-compariosn of POLDER-3 PDL and GRASP products

To have an overview of the performance and robustness of PDL algorithm at regional scales, we examine the annual map of POLDER-3 PDL retrievals during 2008 and make an inter-comparison with GRASP products (Fig. 8). Spatial distribution of PDL aerosol parameters in eastern China have very self-consistent patterns with anthropogenic emission sources and topography. The PDL AOD and SSA have a high consistency with GRASP/Models retrievals that have their best performance in validations with AERONET inversions. The high values of PDL coarse AOD in Gobi deserts agree well with the hotspots of dust activities (Tao and Chen, 2022). By contrast, GRASP/HP and Models tend to overestimate the coarse AOD and GARSP/Models also underestimate the fine AOD, which exhibit lower accuracy than GRASP/Component (Fig. 6). On the other hand, GRASP/Models SSA at 670 nm is around 0.95 and 0.80 in the Gobi deserts and southeast coastal area respectively, where PDL SSA is ~0.90. The notable differences between PDL and GRASP SSA values in clean background regions can be caused by their retrieval errors and distinct constraints in condition of low information content. Additionally, PDL retrievals over the coastlines of eastern China are less influenced by bright surface of the shallows.

Moreover, the spatial patterns of PODER-3 PDL and GRASP retrievals are very consistent in seasonal scales (Fig. 9). PDL fine AOD during spring 2008 reveals a few hotspots of urban emissions ove large cities such as ShijiaZhuang and Zhengzhou in northern China. Owing to the overestimation of coarse AOD for GRASP/HP and Models, PDL and GRASP/Component AOD agree better in northern China. While PDL coarse AOD gets lower from north to south, GRASP/Component retrievals have several high-value (>0.4) areas in central China and the Sichuan Basin. Moreover, PDL coarse AOD over Gobi deserts is closer with GRASP/HP retrieval. All GRASP coarse AODs exhibit an obvious

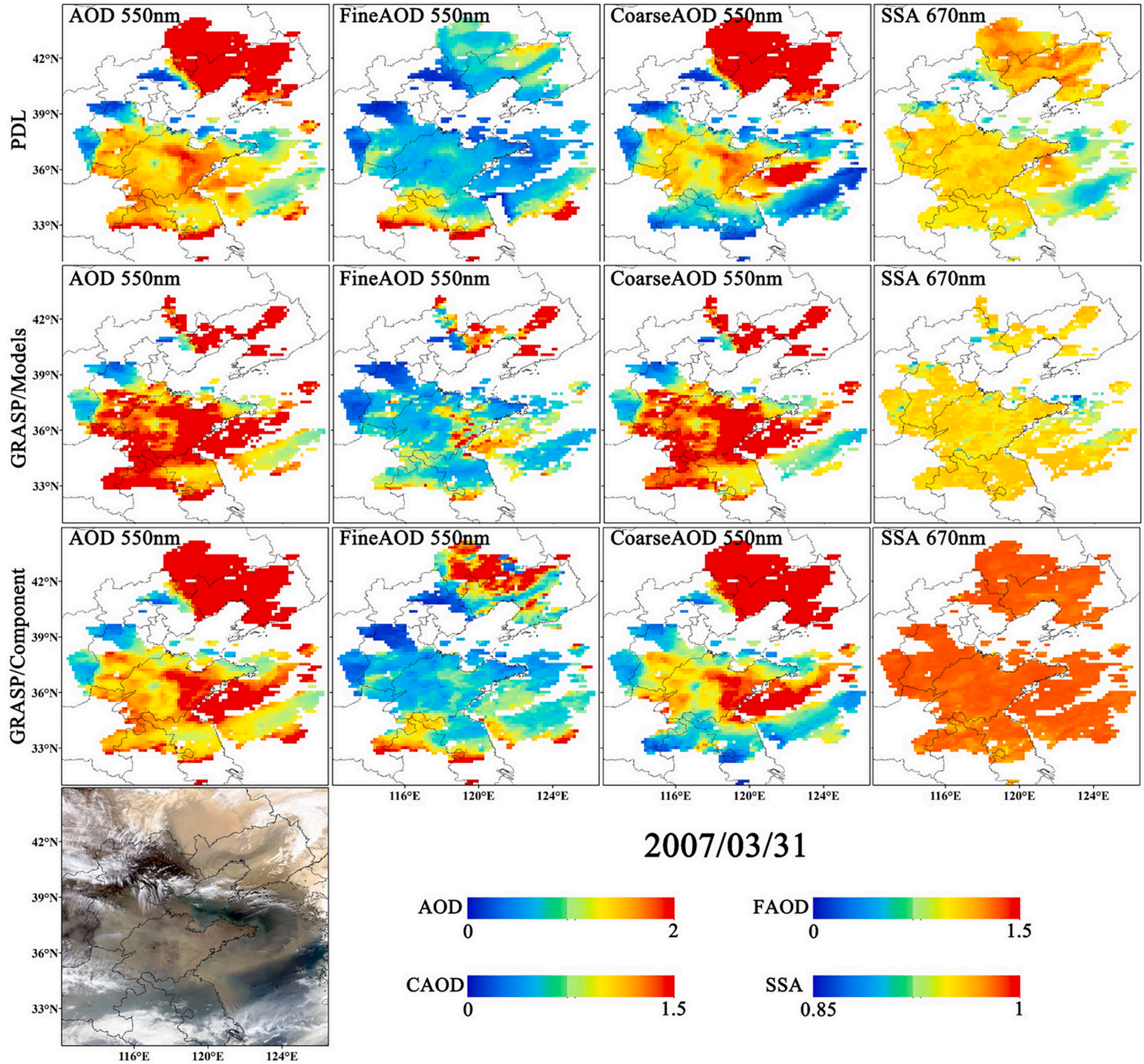

Fig. 10. POLDER-3 AOD, fine AOD, coarse AOD at 550 nm, and SSA at 670 nm for PDL (top), GRASP/Models (middle), and GRASP/Component (bottom) in northern China on March 31, 2007.

overestimation over eastern China during summer (Fig. 1S), due largely to their different assumptions.

To further check the stability of PDL retrievals, a typical dust event over northern China on March 31, 2007 is analyzed (Fig. 10). The POLDER-3 PDL aerosol products can well capture spatial distribution of the dust plumes. Moreover, PDL retrievals can clearly discriminate dust plumes dominated by coarse particles and haze pollution in the southern part with high values of fine AOD. Spatial variations of coarse AOD from PDL in northern China show that the main part of dust plumes has moved to the Yellow sea. Compared with the dense dust plumes in northeastern China with high PDL SSA values around 0.95, absorption of the dust particles over northern China gets stronger with lower PDL SSA at ~0.92, which can be caused by dust-pollution mixing.

For the detection ability of aerosol absorption, we examine PDL retrievals in a biomass burning event in northern China on May 28, 2007 (Fig. 11). The agricultural straw fires during the harvest season emit large amounts of smoke, and have been blown northeasterly by the airflows. Similar as GRASP/Models and Component products, PDL SSA at 670 nm exhibits very low values around 0.80–0.85 over the fire emissions. However, PDL SSA values quickly go up to 0.90–0.95 in the transport, due possibly to a mixture with other anthropogenic emissions and aging of the fresh smoke. In addition, GRASP products tend to overestimate the coarse AOD of the fire smoke.

4.3. *Application potential and uncertainties of the PDL algorithm*

The PDL method has a a robust and reliable performance in ground validation and inter-comparsion with GRASP retrievals. By combining the physical constraint from RT simulations and modeling ability of DL methods, PDL can model the whole MAP measurements with each interested aerosol/surface parameter individually. Thus, PDL method can not only make full use of the observation information, but also avoid

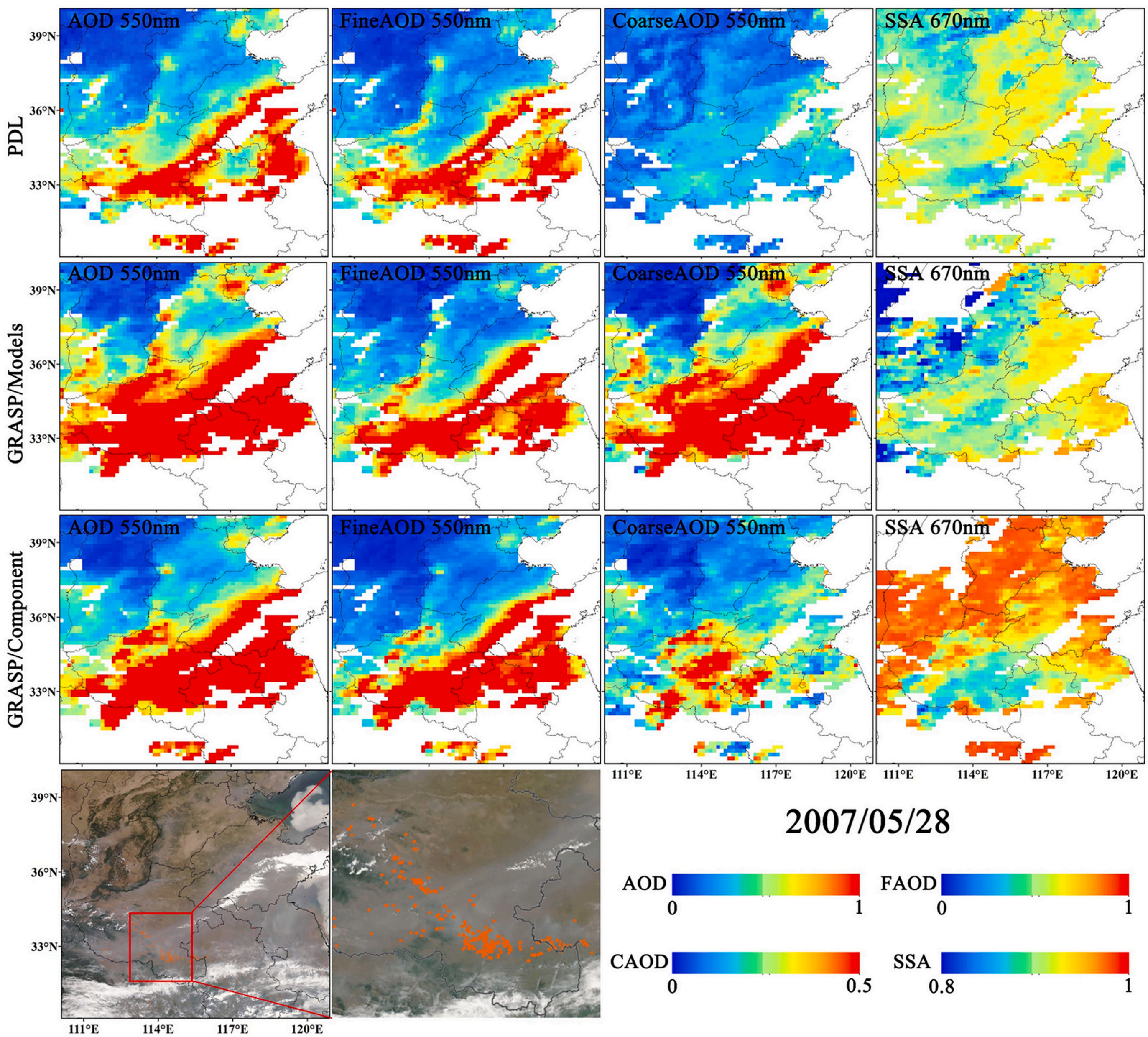

Fig. 11. Same as Fig. 10 but for May 28, 2007.

error propagation among aerosol/surface parameters with different information content in iterative RT calculations. Moreover, PDL can well take advantage of the prior information from existing ground-based observations and satellite surface products. The flexible framework of PDL supports a free selection of retrieved parameters and be applied to other satellite instruments conveniently by making corresponding RT simulations,

Since RT simulation is only needed in the pre-training stage once for each atmosphere/surface scenario, PDL retrievals avoids time-consuming iterative RT calculations for each satellite pixel. By taking satellite measurements as input variables of the trained DBN model, PDL retrievals have a very high computational efficiency. For instance, POLDER PDL aerosol retrievals of one cloud-free image can be implemented at one minute level by using common PC. Compared with the multi-pixel GRASP retrievals, PDL results derived from single-pixel measurement can reflect finer features such as small urban/industrial hotspots in northern China (Fig. 12).

Although accuracy of POLDER-3 PDL AOD and fine AOD is very close to that of the retrievals from test dataset (Fig. 4), coarse AOD and SSA still have considerable uncertainties. Considering the similar performance of GRASP inversions, the limited information content from POLDER-3 measurements could be the main reason (Dong et al., 2023). For PDL SSA, the high values of retrieval bias are concentrated in low-AOD (<0.5) conditions (Fig. 2S), when information content is not sufficient for accurate retrieval of aerosol absorption. To introduce prior constraints such as known aerosol types with fixed complex refractive index in GRASP/Models can be a favor. POLDER-3 PDL AOD has slight overestimation at low values (<0.2), which can be partly caused by the positive bias of coarse AOD (Figs. 5 and 6). Also, high values (>1.0) of PDL AOD become obviously scattered, indicating that aerosol microphysical properties at high AOD are not well characterized in the training. The optimized inversions such as GRASP can quantify reliability or quality of each retrieval by their residual errors in fitting satellite measurements (Dubovik et al., 2021). By contrast, evaluation of uncertainties in PDL retrievals is done in the pre-training stage and focuses on performance of the whole trained model rather than single

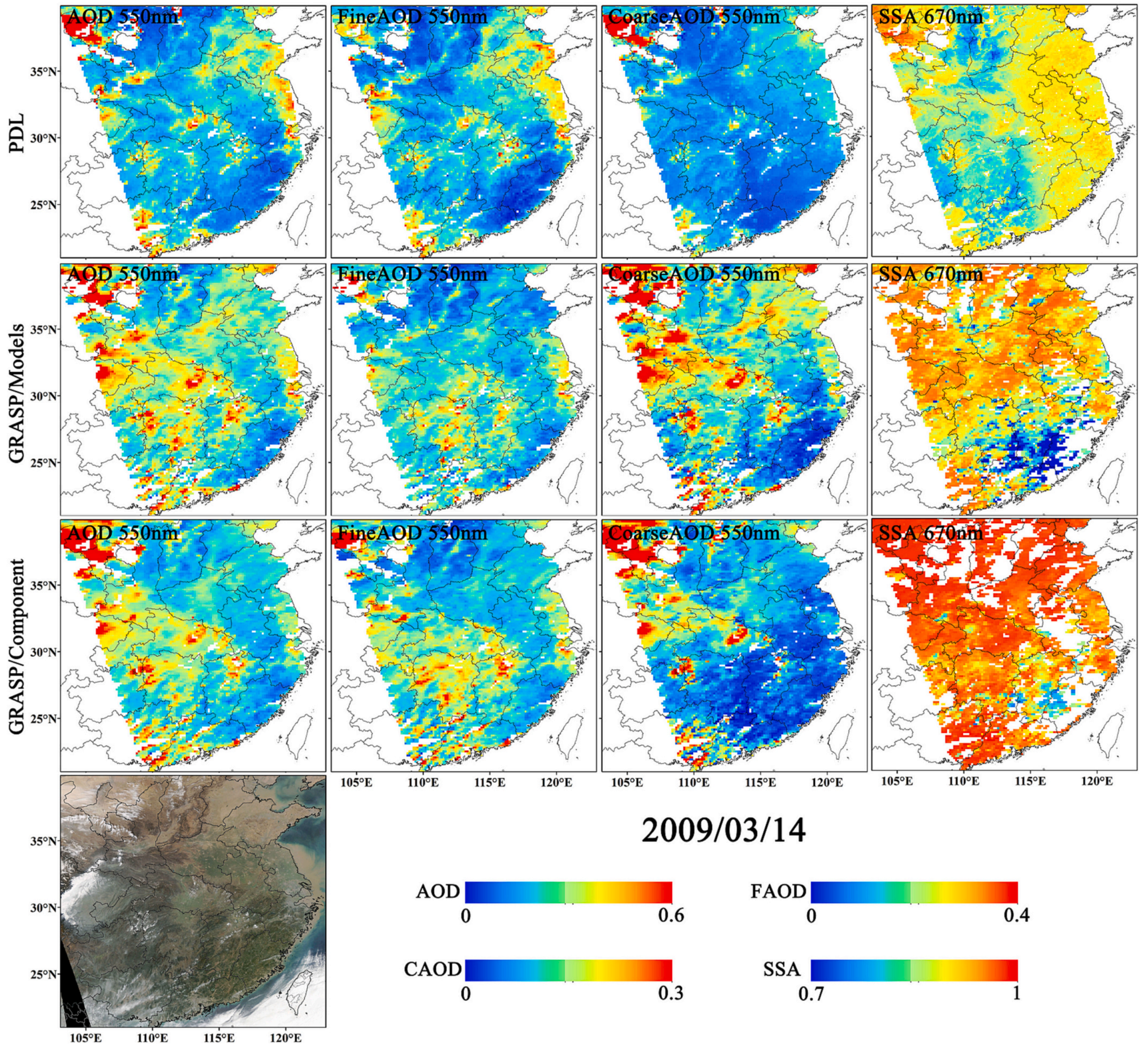

Fig. 12. Same as Fig. 10 but for March 14, 2009.

retrieval.

As an exploratory study, we test and validate the POLDER-3 PDL retrievals only in eastern China. There are still a few of limitations in the PDL method that need to be improved and perfected before a wide application. First, the uncertainties of PDL retrievals could increase in unusual cases or aerosol scenarios such as heavy pollution that only account for a small proportion in all the observations, which should be fully considered in the PDL training. To expand PDL retrievals to lager scales, current training based on aerosol properties in eastern China can have few typical aerosol scenarios such as wildfire smoke and dust events in other regions of the world. Global AERONET climatology of distinct aerosol types such as in GRASP/Models algorithm is needed for the training. Also, the forward RT model we used for generating training datasets did not consider the non-spherical shape of coarse particles. AERONET validation show no obvious changes in the performance of PDL retrievals during the dusty season in northern China (Fig. 3S). The influence of spherical assumption for coarse aerosols can be largely eliminated by DL modeling and spectral and angular information. However, it's still necessary to utilize a more accurate spheroid model in the future work. Additionally, satellite surface BRDF can have non-negligible bias at large viewing angles (Litvinov et al., 2011; Tao et al., 2019). Motivated by the flexible framework, reliable performance, and very high computational efficiency of PDL method, we will refine the current model to apply to more satellite measurements and larger scales in the follow-up study.

5. Conclusions

The emerging MAP satellite measurements have put forward higher demands for efficient retrieval algorithms. In this study, we developed a flexible and high-efficiency algorithm framework for retrieval of aerosol optical/microphysical parameters from MAP measurements with physics-informed deep learning (PDL) method. Unlike the optimized inversion needs iterative RT calculations of all the unknowns together, the PDL method can model the whole MAP observations with interested aerosol parameters separately with the pre-training of RT simulations.

Besides an efficient utilization of satellite observations, PDL retrievals avoid error propagation among aerosol/surface parameters with different information content in optimized inversions. Moreover, the training of PDL can effectively utilize the existing prior information of satellite products and ground-based observations, which can provide a constraint of unphysical values.

Ground-based validations with AERONET products show high accuracy of POLDER-3 PDL AOD and fine AOD in eastern China with higher R (>0.91) and lower RMSE than GRASP retrievals. Owing to overestimation in low values (<0.2), the percent of PDL AOD (59.71%) within the EE of $\pm(0.05 + 15\%)$ is lower than that of GRASP/Models (64.92%). By contrast, PDL fine and coarse AOD performs obviously better than GRASP retrievals. Despite lower accuracy than AOD, PDL SSA is consistent with AERONET inversions and very close to the best estimates from GRASP/Models. By quantifying particle size and absorption, POLDER-3 PDL retrievals can well characterize the spatial distribution and transport process of typical dust and biomass burning events. With a robust performance in accuracy and efficiency, the flexible PDL algorithm has an outstanding potential for operational retrieval of MAP satellite measurements. To apply PDL method to more satellite measurements and larger scales, we will refine the PDL method by enhancing prior constraints and improving RT simualtions in the following study.

CRediT authorship contribution statement

Minghui Tao: Conceptualization, Writing – original draft. **Jinxi Chen:** Methodology. **Xiaoguang Xu:** Investigation. **Wenjing Man:** Visualization. **Lina Xu:** Supervision, Writing – review & editing. **Lunche Wang:** Data curation. **Yi Wang:** Formal analysis. **Jun Wang:** Software. **Meng Fan:** Validation. **Muhammad Imran Shahzad:** Resources. **Liangfu Chen:** Project administration.

Declaration of Competing Interest

The authors declare the following financial interests/personal relationships which may be considered as potential competing interests: Minghui Tao reports a relationship with National Natural Science Foundation of China that includes: funding grants.

Data availability

Data will be made available on request.

Acknowledgments

This study was supported by National Natural Science Foundation of China (Grant No. 41830109 and 42271382). We thank the POLDER (https://www.icare.univ-lille1.fr/) and GRASP team (https://www.grasp-open.com/) for the satellite data used in our work. Thanks for Dr. Li Lei for the discussion regrading GRASP products. We acknowledge AERONET site PIs (B.N. Holben, H. Chen, L. Wu, R. Ma, J.E. Nichol, P. Wang, X. Xia, and Z. Li) for providing the aerosol data available.

Appendix A. Supplementary data

Supplementary data to this article can be found online at https://doi.org/10.1016/j.rse.2023.113763.

References

Chen, C., Dubovik, O., et al., 2020. Validation of GRASP algorithm product from POLDER/PARASOL data and assessment of multi-angular polarimetry potential for aerosol monitoring. Earth Syst. Sci. Data 12 (4), 3573–3620.
Chen, C., Dubovik, O., et al., 2022a. Multi-angular polarimetric remote sensing to pinpoint global aerosol absorption and direct radiative forcing. Nat. Commun. 13 (1), 7459.
Diner, D.J., Boland, S.W., Brauer, M., et al., 2018. Advances in multiangle satellite remote sensing of speciated airborne particulate matter and association with adverse health effects: from MISR to MAIA. J. Appl. Remote. Sens. 12 (4), 042603.
Chen, X., Wang, J., et al., 2022b. Analytical prediction of scattering properties of spheroidal dust particles with machine learning. Geophys. Res. Lett. 49 (9), e2021GL097548.
Di Noia, A., Hasekamp, O.P., et al., 2015. Use of neural networks in ground-based aerosol retrievals from multi-angle spectropolarimetric observations. Atmos. Meas. Tech. 8 (1), 281–299.
Di Noia, A., Hasekamp, O.P., et al., 2017. Combined neural network/Phillips–Tikhonov approach to aerosol retrievals over land from the NASA research scanning polarimeter. TmosMeas. Tech. 10 (11), 4235–4252.
Dong, W., Tao, M., et al., 2023. Satellite aerosol retrieval from multi-angle polarimetric measurements: information content and uncertainty analysis. IEEE Trans. Geosci. Remote Sens. 61, 1–13.
Dubovik, O., Herman, M., Holdak, A., Lapyonok, T., Tanré, D., Deuzé, J., Ducos, F., Sinyuk, A., Lopatin, A., 2011. Statistically optimized inversion algorithm for enhanced retrieval of aerosol properties from spectral multi-angle polarimetric satellite observations. Atmos. Measur. Techn 4 (5), 975.
Dubovik, O., et al., 2019. Polarimetric remote sensing of atmospheric aerosols: instruments, methodologies, results, and perspectives. J. Quant. Spectrosc. Radiat. Transf. 224, 474–511.
Dubovik, O., Fuertes, D., et al., 2021. A comprehensive description of multi-term LSM for applying multiple a priori constraints in problems of atmospheric remote sensing: GRASP algorithm, concept, and applications. Front. Remote Sens. 2 (23).
Dubovik, O., Holben, B., et al., 2002. Variability of Absorption and Optical Properties of Key Aerosol Types Observed in Worldwide Locations. J. Atmos. Sci. 59 (3), 590–608.
Forster, P., Storelvmo, T., Armour, K., Collins, W., Dufresne, J.-L., Frame, D., Lunt, D.J., Mauritsen, T., Palmer, M.D., Watanabe, M., Wild, M., Zhang, H., 2021. The Earth's energy budget, climate feedbacks, and climate sensitivity.. In: Climate Change 2021: The Physical Science Basis. Contribution of Working Group I to the Sixth Assessment Report of the Intergovernmental Panel on Climate Change. Cambridge University Press, Cambridge, United Kingdom and New York, NY, USA, pp. 923–1054. https://doi.org/10.1017/9781009157896.009.
Fougnie, B., Marbach, T., et al., 2018. The multi-viewing multi-channel multi-polarisation imager–overview of the 3MI polarimetric mission for aerosol and cloud characterization. J. Quant. Spectrosc. Radiat. Transf. 219, 23–32.
Fu, G., Hasekamp, O., 2018. Retrieval of aerosol microphysical and optical properties over land using a multimode approach. Atmos. Meas. Tech. 11 (12), 6627–6650.
Gao, M., Franz, B.A., et al., 2021. Efficient multi-angle polarimetric inversion of aerosols and ocean color powered by a deep neural network forward model. Atmos. Meas. Tech. 14 (6), 4083–4110.
Giles, D.M., Sinyuk, A., et al., 2019. Advancements in the aerosol robotic network (AERONET) version 3 database – automated near-real-time quality control algorithm with improved cloud screening for sun photometer aerosol optical depth (AOD) measurements. Atmos. Meas. Tech. 12 (1), 169–209.
Hasekamp, O.P., Litvinov, P., Butz, A., 2011. Aerosol properties over the ocean from PARASOL multiangle photopolarimetric measurements. J. Geophys. Res. 116, D14204. https://doi.org/10.1029/2010JD015469.
Hinton, G.E., Osindero, S., et al., 2006. A fast learning algorithm for deep belief nets. Neural Comput. 18 (7), 1527–1554.
Holben, B.N., et al., 1998. AERONET—A federated instrument network and data archive for aerosol characterization. Remote Sens. Environ. 66, 1–16.
Hsu, N.C., Jeong, M.J., Bettenhausen, C., Sayer, A.M., Hansell, R., Seftor, C.S., Huang, J., Tsay, S.C., 2013. Enhanced deep blue aerosol retrieval algorithm: the second generation. J. Geophys. Res. 118 (16), 9296–9315.
Ichoku, C., Chu, D.A., Mattoo, S., Kaufman, Y.J., Remer, L.A., Tanré, D., Slutsker, I., Holben, B.N., 2002. A spatio-temporal approach for global validation and analysis of MODIS aerosol products. Geophys. Res. Lett. 29 (12). MOD1-1-MOD1-4.
Jia, C., Sun, L., et al., 2022. Satellite aerosol retrieval using scene simulation and deep belief network. IEEE Trans. Geosci. Remote Sens. 60, 1–16.
Kahn, R.A., Gaitley, B.J., 2015. An analysis of global aerosol type as retrieved by MISR. J. Geophys. Res. Atmos. 120 (9), 4248–4281.
Kang, Y., Kim, M., et al., 2022. Improved retrievals of aerosol optical depth and fine mode fraction from GOCI geostationary satellite data using machine learning over East Asia. ISPRS J. Photogramm. Remote Sens. 183, 253–268.
Kaufman, Y.J., Tanre, D., Boucher, O., 2002. A satellite view of aerosols in the climate system. Nature 419 (6903), 215–223.
King, M.D., Kaufman, Y.J., Tanré, D., Nakajima, T., 1999. Remote sensing of tropospheric aerosols from space: past, present, and future. Bull. Am. Meteorol. Soc. 80 (11), 2229–2259.
Levy, R.C., Mattoo, S., Munchak, L.A., Remer, L.A., Sayer, A.M., Patadia, F., Hsu, N.C., 2013. The collection 6 MODIS aerosol products over land and ocean. Atmos. Measur. Techn. 6 (11), 2989–3034.
Li, L., Dubovik, O., Derimian, 2019. Retrieval of aerosol components directly from satellite and ground-based measurements. Atmos. Chem. Phys. 19, 13409–13443.
Li, L., Derimian, Y., et al., 2022. Climatology of aerosol component concentrations derived from multi-angular polarimetric POLDER-3 observations using GRASP algorithm. Earth Syst. Sci. Data 14 (7), 3439–3469.
Litvinov, P., Hasekamp, O., et al., 2011. Models for surface reflection of radiance and polarized radiance: comparison with airborne multi-angle photopolarimetric measurements and implications for modeling top-of-atmosphere measurements. Remote Sens. Environ. 115 (2), 781–792.
Lucht, W., Schaaf, C.B., et al., 2000. An algorithm for the retrieval of albedo from space using semiempirical BRDF models. IEEE Trans. Geosci. Remote Sens. 38 (2), 977–998.

Lyapustin, A., Wang, Y., et al., 2018. MODIS collection 6 MAIAC algorithm. Atmos. Meas. Tech. 11 (10), 5741–5765.
Maignan, F., Bréon, F.-M., et al., 2009. Polarized reflectances of natural surfaces: spaceborne measurements and analytical modeling. Remote Sens. Environ. 113 (12), 2642–2650.
Pope, I.C., Burnett, R.T., Thun, M.J., et al., 2002. Lung cancer, cardiopulmonary mortality, and long-term exposure to fine particulate air pollution. J. Am. Med. Assoc. 287 (9), 1132–1141.
Sanghavi, S., Nelson, R., et al., 2020. Aerosols in OCO-2/GOSAT retrievals of XCO2: an information content and error analysis. Remote Sens. Environ. 251, 112053.
Shi, C., Hashimoto, M., et al., 2020. Development of an algorithm to retrieve aerosol optical properties over water using an artificial neural network radiative transfer scheme: first result from GOSAT-2/CAI-2. IEEE Trans. Geosci. Remote Sens. 1–12.
Sinyuk, A., Holben, B.N., et al., 2020. The AERONET version 3 aerosol retrieval algorithm, associated uncertainties and comparisons to version 2. Atmos. Meas. Tech. 13 (6), 3375–3411.
Tanré, D., Bréon, F.M., et al., 2011. Remote sensing of aerosols by using polarized, directional and spectral measurements within the A-train: the PARASOL mission. Atmos. Meas. Tech. 4 (7), 1383–1395.
Tao, M., Wang, J., Li, R., Wang, L., Wang, L., Wang, Z., Tao, J., Che, H., Chen, L., 2019. Performance of MODIS high-resolution MAIAC aerosol algorithm in China: characterization and limitation. Atmos. Environ. 213, 159–169.
Tao, M., Chen, L., et al., 2022. Characterization of dust activation and their prevailing transport over East Asia based on multi-satellite observations. Atmos. Res. 265, 105886.
Tao, M., Wang, J., et al., 2020. Characterization of aerosol type over East Asia by 4.4 km MISR product: first insight and general performance. J. Geophys. Res. Atmos. 125 (13) e2019JD031909.
Waquet, F., Cairns, B., Knobelspiesse, K., Chowdhary, J., Travis, L.D., Schmid, B., Mishchenko, M.I., 2009. Polarimetric remote sensing of aerosols over land. J. Geophys. Res. 114, D01206. https://doi.org/10.1029/2008JD010619.
Wang, J., Xu, X., et al., 2014. A numerical testbed for remote sensing of aerosols, and its demonstration for evaluating retrieval synergy from a geostationary satellite constellation of GEO-CAPE and GOES-R. J. Quant. Spectrosc. Radiat. Transf. 146, 510–528.
Xu, F., van Harten, G., Diner, D.J., Kalashnikova, O.V., Seidel, F.C., Bruegge, C.J., Dubovik, O., 2017. Coupled retrieval of aerosol properties and land surface reflection using the airborne multiangle SpectroPolarimetric imager. J. Geophys. Res. Atmos. 122 (13), 7004–7026.
Xu, X., Wang, J., 2015a. Retrieval of aerosol microphysical properties from AERONET photopolarimetric measurements: 1. Information content analysis. J. Geophys. Res. Atmos. 120 (14), 7059–7078.
Xu, X., Wang, J., et al., 2015b. Retrieval of aerosol microphysical properties from AERONET photopolarimetric measurements: 2. A new research algorithm and case demonstration. J. Geophys. Res. Atmos. 120 (14), 7079–7098.
Zhang, X., Li, L., et al., 2021. Validation of the aerosol optical property products derived by the GRASP/Component approach from multi-angular polarimetric observations. Atmos. Res. 263, 105802.